

State Estimation for the discretized LWR PDE using explicit polyhedral representations of the Godunov scheme

JEROME THAI

BORIS PRODHOMME

ALEXANDRE M. BAYEN

Abstract—This article investigates the problem of estimating the state of discretized hyperbolic scalar partial differential equations. It uses a Godunov scheme to discretize the so-called *Lighthill-Whitham-Richards* equation with a triangular flux function, and proves that the resulting nonlinear dynamical system can be decomposed in a *piecewise affine* manner. Using this explicit representation, the system is written as a switching dynamical system (hybrid system), with an exponential number of modes. The estimation problem is posed using *Kalman filtering* in each of the linear mode, and the approach becomes computationally tractable by tracking the mode evolution as the estimation is performed at each time step. Numerical results are presented using the *Mobile Millennium* data set, and compared to results obtained using *ensemble Kalman filtering*, which is used for estimation in traffic monitoring.

I. INTRODUCTION

Numerous traffic estimation techniques developed in the literature rely on density-based traffic models such as the *Lighthill-Whitham-Richards* (LWR) partial differential equation (PDE) [19], [23] and its discretization using the *Godunov scheme* [15], [18], [25] also known as the *Cell Transmission Model* (CTM) [6], [7] in the transportation literature. Highway traffic monitoring systems which rely on these models use large amounts of data from different sources. These include *inductive loop detectors* (ILD) such as the ones used in the PeMS system [4] and *in-vehicle transponders* (IVTs) such as FasTrak. Recently, the amount of available traffic data has increased tremendously since the development of cellular phone based highway traffic monitoring [32]. Large scale applications include traffic flow estimation to assimilate velocity measurements [30], [31]. With this rapid increase in available data, the necessity of using powerful statistical filters and algorithms to efficiently assimilate the measurements has become evident.

In the 70's, Gazis [9], [26] was among the first to use the *Kalman filter* (KF) and the *extended Kalman filter* (EKF) for sequential traffic state estimation. Recently, Papageorgiou [28], [29] applied the EKF to a non-scalar traffic model [22]. The EKF has also been applied to the LWR equation in [24]. In [30], [31] the *ensemble Kalman filter* is used to assimilate velocity measurements. In [21], a *switching-mode model* (SMM) has been derived from the *Cell Transmission Model* (CTM), which is a nonlinear discrete time dynamical

system. This consists in switching among different sets of linear difference equations, defined as linear *state-space model* (SSM) or modes, combined with a hidden Markov model to describe the transitions from one mode to another. The *mixture Kalman filter* algorithm [5] is employed to assimilate data in a switching state-space model. In this article, we show that for a triangular flux function, the Godunov scheme applied to the LWR model (described in [7]) is a *piecewise affine* (PWA) dynamic system, in which each affine component is a mode. Contrary to the SMM, for which an additional statistical model, namely the hidden Markov model, is introduced, we unravel the PWA character of the *Godunov scheme*. Hence, the *Godunov scheme* is a special case of hybrid systems, for which there has been considerable interests in the among researchers in academic and industrial communities [2], [16], [17], [27].

The contribution of this article are as follows:

- An explicit formulation of the *piecewise affine* (PWA) nature of the *Godunov scheme* and a description of the affine components (or modes).
- A hybrid filtering algorithm in which the *Kalman filter* is applied to each mode, which is a special case of EKF.
- An efficient implementation of this filtering algorithm.

The rest of the article is organized as follows: Section II, presents the mathematical model used in the rest of the article. Section III unravels the PWA character of the *Godunov scheme*. Section IV presents a Kalman filter implementation using the PWA character of the *Godunov scheme*, and Section V some numerical results.

II. MATHEMATICAL MODEL

A. The LWR Model

Lighthill, Whitham in 1955 [19], and Richards in 1956 [23] introduced a macroscopic dynamic model of traffic based on conservation of vehicles (II.1), using Greenshields' hypothesis [12] of a static flow/density relationship (II.1), known as the *flux function*:

$$q(x, t) = Q(\rho(x, t)) \quad (\text{II.1})$$

where $\rho(x, t)$ and $q(x, t)$ denote the density and the flow of vehicles at location x and time t respectively, and Q is the flux function which is assumed to be a function of the density only. The conservation of mass can be rewritten as follows:

$$\frac{\partial \rho(x, t)}{\partial t} + \frac{\partial Q(\rho(x, t))}{\partial x} = 0 \quad (\text{II.2})$$

Department of Electrical Engineering and Computer Science, University of California, Berkeley, jerome.thai@berkeley.edu

Assistant Specialist at UC Berkeley Institute of Transportation Studies, Berkeley, boris.prodhomme@polytechnique.edu

Associate Professor, Systems Engineering, Department of Electrical Engineering and Computer Sciences, Department of Civil and Environmental Engineering, University of California, Berkeley, bayen@berkeley.edu

This equation is commonly known as the *Lighthill-Whitham-Richards*, or LWR, model. Different flux functions have been suggested. They all share the same characteristics **LWR1-6**:

LWR1. Greenshields' hypothesis of a static flow/density relationship: $q = Q(\rho(x, t))$

LWR2. $Q(0) = Q(\rho_{\text{jam}}) = 0$ where the jam density ρ_{jam} refers to extreme traffic density associated with completely stopped traffic flow.

LWR3. The continuous portions of $Q(\rho)$ are concave.

LWR4. $V(0) = v_f$, and $V(\rho_{\text{jam}}) = 0$.

LWR5. A critical density ρ_c can be defined in which the maximum flow q_c is attained. Then, $Q(\rho)$ is increasing for $\rho \leq \rho_c$ and decreasing for $\rho > \rho_c$.

LWR6. The critical density ρ_c separates the flux function into two regimes: *free flow* when $\rho \leq \rho_c$ and *congestion* when $\rho > \rho_c$

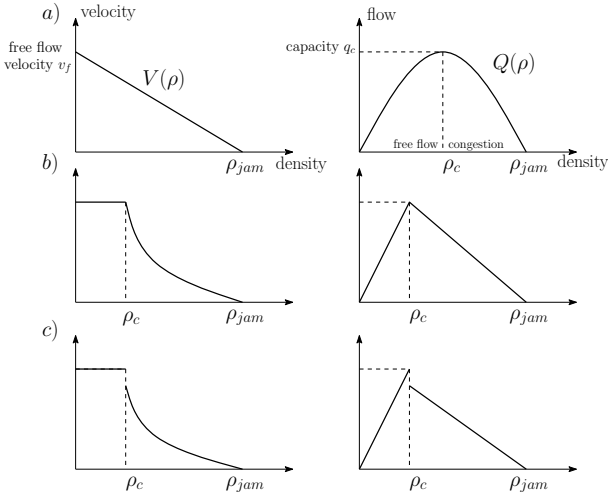


Fig. II.1: Speed and flow relationships for Greenshields (a), triangular (b), and discontinuous (c).

For instance, Greenshields [12] found that freeway speed and density could be reasonably well approximated by an affine function. The widely used triangular velocity function [7] assumes a constant velocity in free-flow and a hyperbolic velocity in congestion as shown in Figure II.1:

$$v = V_T(\rho) = \begin{cases} v_f & \text{if } \rho \leq \rho_c \\ -\omega_f \left(1 - \frac{\rho_{\text{jam}}}{\rho}\right) & \text{if } \rho > \rho_c \end{cases} \quad (\text{II.3})$$

and the corresponding flux function is:

$$Q_T(\rho) = \begin{cases} \rho V_T(\rho) & \\ = \begin{cases} v_f \rho & \text{if } \rho \leq \rho_c \\ -\omega_f (\rho - \rho_{\text{jam}}) & \text{if } \rho > \rho_c \end{cases} \end{cases} \quad (\text{II.4})$$

where $\omega_f = v_f \rho_c / (\rho_{\text{jam}} - \rho_c)$ is the backwards propagation wave speed.

In [1], [3], [13], a *capacity drop* on the order of 4-10% in the peak flow $Q(\rho_c)$ has been proposed, as the freeway transitions into congestion (cf Figure II.1).

B. Numerical Discretization

A seminal numerical method to solve the above equations is given by the Godunov scheme, which is based on exact solutions to Riemann problems [10], [11]. This leads to the construction of a nonlinear discrete time dynamical system. The Godunov discretization scheme is applied on the LWR PDE, where the discrete time step Δt is indexed by t , and the discrete space step Δx is indexed by i :

$$\rho_i^{t+1} = \rho_i^t - \frac{\Delta t}{\Delta x} (G(\rho_i^t, \rho_{i+1}^t) - G(\rho_{i-1}^t, \rho_i^t)) \quad (\text{II.5})$$

In order to ensure numerical stability, the time and space steps are coupled by the CFL condition [18]: $c_{\text{max}} \frac{\Delta t}{\Delta x} \leq 1$ where c_{max} denotes the maximal characteristic speed.

For a family of flux functions $Q(\rho)$ that share the same characteristics **LWR1-6** listed above, the Godunov flux can be expressed as the minimum of the *sending flow* $S(\rho)$ from the upstream cell and the *receiving flow* $R(\rho)$ from the downstream cell (II.7, II.8, II.9) through a boundary connecting two cells of a homogeneous road (i.e. the upstream and downstream cells have the same characteristics).¹ For the triangular flux function:

$$G(\rho_1, \rho_2) = \min(S(\rho_1), R(\rho_2)) \quad (\text{II.7})$$

$$S(\rho) = \begin{cases} Q(\rho) = v_f \rho & \text{if } \rho \leq \rho_c \\ q_c & \text{if } \rho > \rho_c \end{cases} \quad (\text{II.8})$$

$$R(\rho) = \begin{cases} q_c & \text{if } \rho \leq \rho_c \\ Q(\rho) = -\omega_f (\rho - \rho_{\text{jam}}) & \text{if } \rho > \rho_c \end{cases} \quad (\text{II.9})$$

where ρ_1 is the density of the cell upstream and ρ_2 is the density of the cell downstream.

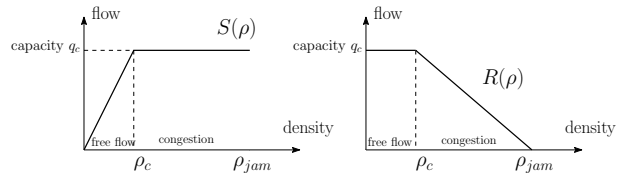


Fig. II.2: Sending and receiving flows for triangular velocity function.

As shown in Figure II.2, the application of the Godunov scheme to the flux functions introduces intuitive concepts of *supply* and *demand* at the boundary connecting two cells. The upstream cell supplies the flow at the boundary up to capacity. On the other hand, when the downstream traffic is congested, there is a decrease in demand from the downstream cell, limiting the flow through the boundary.

¹There are various definitions of the Godunov flux $G(\rho_1, \rho_2)$ in the literature, notably in [8]:

$$G(\rho_1, \rho_2) = \begin{cases} \min_{\rho \in [\rho_1, \rho_2]} Q(\rho) & \text{if } \rho_1 \leq \rho_2 \\ \max_{\rho \in [\rho_2, \rho_1]} Q(\rho) & \text{if } \rho_2 \leq \rho_1 \end{cases} \quad (\text{II.6})$$

This assumes that a flux function is defined at each boundary between two cells.

Important remark: For the rest of the article, the widely-used *triangular flux function* described in [6] is chosen for our dynamic model and results are derived from it. We also assume for simplicity and clarity that the segment of road we are modelling is homogeneous, i.e. the parameters of the flux function $\omega_f, v_f, \rho_{\text{jam}}, \rho_c, q_c$ are uniform along the cells of the discretized road. All the results derived in the rest of the article still remain valid for an heterogeneous road, in particular the piecewise affine character of the model and the tractability of the Kalman filter algorithm, but the number of modes and the complexity increase.

The explicit values taken by $G(\rho_1, \rho_2)$ for a partition of the space in different regions of the space (ρ_1, ρ_2) **W**, **L**, and **D** are shown in Figure II.3 and defined by equations II.11. In the triangular case:

$$G_T(\rho_1, \rho_2) = \begin{cases} R(\rho_2) = -\omega_f(\rho_2 - \rho_{\text{jam}}) & \text{if } (\rho_1, \rho_2) \in \mathbf{W} \\ q_c & \text{if } (\rho_1, \rho_2) \in \mathbf{L} \\ S(\rho_1) = v_f \rho_1 & \text{if } (\rho_1, \rho_2) \in \mathbf{D} \end{cases} \quad (\text{II.10})$$

$$\begin{aligned} \mathbf{W} &= \{(\rho_1, \rho_2) \mid \rho_2 > h(\rho_1), \rho_2 > \rho_c\} \\ \mathbf{L} &= \{(\rho_1, \rho_2) \mid \rho_1 > \rho_c, \rho_2 \leq \rho_c\} \\ \mathbf{D} &= \{(\rho_1, \rho_2) \mid \rho_2 \leq h(\rho_1), \rho_1 \leq \rho_c\} \end{aligned} \quad (\text{II.11})$$

The boundary between the **W** and **D** regions follows the $(\rho_1, \rho_2) = (\rho_1, h(\rho_1))$ trajectory for $\rho_1 \leq \rho_c$, with:²

$$h(\rho_1) = \bar{R}^{-1}(\bar{S}(\rho_1)) = -\frac{v_f}{\omega_f} \rho_1 + \rho_{\text{jam}} \quad (\text{II.12})$$

where \bar{S} and \bar{R} respectively denote the restrictions of the sending and receiving flows S and R to the sub-regions $[0, \rho_c]$ and $(\rho_c, \rho_{\text{jam}}]$ respectively, which also correspond to the left and right parts of the flux function (w.r.t. ρ_c), as shown in Figure II.3. In the triangular case, **W**, **L**, **D** form a *polyhedral partition* of the space (ρ_1, ρ_2) :

$$\begin{aligned} \mathbf{W} &= \{(\rho_1, \rho_2) \mid \rho_2 + \frac{v_f}{\omega_f} \rho_1 > \rho_{\text{jam}}, \rho_2 > \rho_c\} \\ \mathbf{L} &= \{(\rho_1, \rho_2) \mid \rho_1 > \rho_c, \rho_2 \leq \rho_c\} \\ \mathbf{D} &= \{(\rho_1, \rho_2) \mid \rho_2 + \frac{v_f}{\omega_f} \rho_1 \leq \rho_{\text{jam}}, \rho_1 \leq \rho_c\} \end{aligned} \quad (\text{II.13})$$

III. POLYHEDRAL PIECEWISE AFFINE MODEL

In the Godunov scheme (II.5), the update of the density ρ_i^{t+1} at cell i depends on the triplet $(\rho_{i-1}^t, \rho_i^t, \rho_{i+1}^t)$. With $\frac{\Delta t}{\Delta x} = \alpha$, the Godunov scheme reads:

$$\rho_i^{t+1} = \rho_i^t - \alpha (G(\rho_i^t, \rho_{i+1}^t) - G(\rho_{i-1}^t, \rho_i^t)) \quad (\text{III.1})$$

²Here, we suppose that \bar{R} is a strictly monotonic function on $(\rho_c, \rho_{\text{jam}}]$, hence invertible, and \bar{R}^{-1} denotes its inverse, which is the case for the triangular flux function.

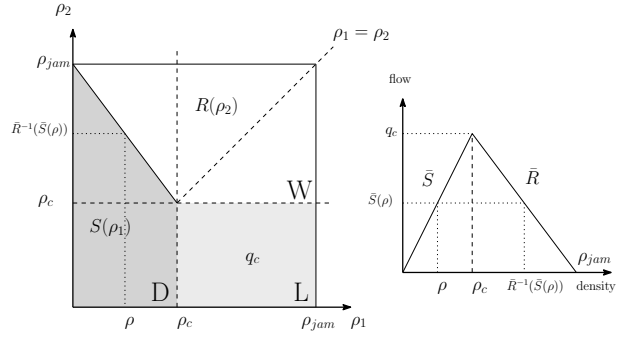


Fig. II.3: Values of $G(\rho_1, \rho_2)$ in the space (ρ_1, ρ_2) .

A. Modal description of the Godunov scheme

The density ρ_i^{t+1} depends on whether both pairs (ρ_{i-1}^t, ρ_i^t) and (ρ_i^t, ρ_{i+1}^t) are in **W**, **L**, or **D** via $G(\rho_{i-1}^t, \rho_i^t)$ and $G(\rho_i^t, \rho_{i+1}^t)$. There are nine possible combinations at cell i , which can be reduced to seven “modes” since the pairs (ρ_{i-1}^t, ρ_i^t) and (ρ_i^t, ρ_{i+1}^t) have ρ_i^t in common. Let us denote by $f(\rho_{i-1}^t, \rho_i^t, \rho_{i+1}^t)$ and $f_T(\rho_{i-1}^t, \rho_i^t, \rho_{i+1}^t)$ the vector functions for the possible values of ρ_i^{t+1} for the general and the triangular cases respectively, for which the variables are ρ_{i-1}^t, ρ_i^t , and ρ_{i+1}^t . Table III.1 list these seven possibilities, which can easily be derived from Figure II.3.

Mode	(ρ_{i-1}^t, ρ_i^t)	(ρ_i^t, ρ_{i+1}^t)	$f(\rho_{i-1}^t, \rho_i^t, \rho_{i+1}^t)$
1	W	W	$\rho_i^t - \alpha(R(\rho_{i+1}^t) - R(\rho_i^t))$
2	W	L	$\rho_i^t - \alpha(q_c - R(\rho_i^t))$
3	L	W	$\rho_i^t - \alpha(R(\rho_{i+1}^t) - q_c)$
4	L	D	$\rho_i^t - \alpha(S(\rho_i^t) - q_c)$
5	D	W	$\rho_i^t - \alpha(R(\rho_{i+1}^t) - S(\rho_{i-1}^t))$
6	D	L	$\rho_i^t - \alpha(q_c - S(\rho_{i-1}^t))$
7	D	D	$\rho_i^t - \alpha(S(\rho_i^t) - S(\rho_{i-1}^t))$

TABLE III.1: 7×1 -dimensional column vector $f(\rho_{i-1}^t, \rho_i^t, \rho_{i+1}^t)$ of the different values of ρ_i^{t+1} depending on the mode.

Mode	$f_T(\rho_{i-1}^t, \rho_i^t, \rho_{i+1}^t)$
1	$(1 - \alpha\omega_f)\rho_i^t + \alpha\omega_f\rho_{i+1}^t$
2	$(1 - \alpha\omega_f)\rho_i^t + \alpha\omega_f\rho_c$
3	$\rho_i^t + \alpha\omega_f\rho_{i+1}^t - \alpha\omega_f\rho_c$
4	$(1 - \alpha v_f)\rho_i^t + \alpha v_f\rho_c$
5	$\alpha v_f\rho_{i-1}^t + \rho_i^t + \alpha\omega_f\rho_{i+1}^t - \alpha\omega_f\rho_{\text{jam}}$
6	$\alpha v_f\rho_{i-1}^t + \rho_i^t - \alpha v_f\rho_c$
7	$\alpha v_f\rho_{i-1}^t + (1 - \alpha v_f)\rho_i^t$

TABLE III.2: 7×1 -dimensional column vector $f_T(\rho_{i-1}^t, \rho_i^t, \rho_{i+1}^t)$ of the different values of ρ_i^{t+1} depending on the mode.

For example, for the first mode, (ρ_{i-1}^t, ρ_i^t) and (ρ_i^t, ρ_{i+1}^t) are both in **W** (see Figure II.3), thus $G(\rho_{i-1}^t, \rho_i^t) = R(\rho_i^t)$ and $G(\rho_i^t, \rho_{i+1}^t) = R(\rho_{i+1}^t)$, and then $\rho_i^{t+1} = \rho_i^t - \alpha(R(\rho_{i+1}^t) - R(\rho_i^t))$. By extending this result to an entire link with discrete state space indexed by $i = 1, \dots, n$, where n is the number of space steps, we have an exhaustive description of the space of “modes” along the link.

Computational complexity: A priori, the number of modes in Table III.1 renders the approach of mode decomposition for estimation untractable: for n cells, the number of possible modes at any given time is equal to 7^n . Since there is a correlation between two consecutive indices i and $i + 1$, the number of modes for the entire link reduces from 7^n to an expression in the form of $a \cdot \beta^n + b \cdot \gamma^n + c \cdot \delta^n$ which lower and upper bounds are proved to be $3 \cdot 2^n$ and $3 \cdot (2.5)^n$ respectively (for full details, see Appendix). And we will see later in section IV-B that the implementation of the Kalman filter in each mode has $O(n^2)$ time complexity and $O(n)$ space complexity.

We define J , the Jacobian matrix of f with respect to $(\rho_{i-1}^t, \rho_i^t, \rho_{i+1}^t)$ in each of the modes (which are all linear):

$$J = \left(\frac{\partial f_j}{\partial \rho_k} \right)_{j=1, \dots, 7, k=i-1, i, i+1} \quad (\text{III.2})$$

Where f_j is the j -th entry of the vector function f defined in Table III.1. It is useful to make the Jacobian matrix J_T of the vector function f_T explicit with respect to $(\rho_{i-1}^t, \rho_i^t, \rho_{i+1}^t)$, and the constant term w :

$$J_T = \begin{pmatrix} 0 & 1 - \alpha\omega_f & \alpha\omega_f \\ 0 & 1 - \alpha\omega_f & 0 \\ 0 & 1 & \alpha\omega_f \\ 0 & 1 - \alpha v_f & 0 \\ \alpha v_f & 1 & \alpha\omega_f \\ \alpha v_f & 1 & 0 \\ \alpha v_f & 1 - \alpha v_f & 0 \end{pmatrix}, w = \begin{pmatrix} 0 \\ \alpha\omega_f \rho_c \\ -\alpha\omega_f \rho_c \\ \alpha v_f \rho_c \\ -\alpha\omega_f \rho_{\text{jam}} \\ -\alpha v_f \rho_c \\ 0 \end{pmatrix} \quad (\text{III.3})$$

Since f_T is a *linear function* of $(\rho_{i-1}^t, \rho_i^t, \rho_{i+1}^t)$ as shown in Table III.1, we can notice that J_T is constant. More notably, the state ρ_i^{t+1} can be rewritten as:

$$f_T(\rho_{i-1}^t, \rho_i^t, \rho_{i+1}^t) = J_T \begin{pmatrix} \rho_{i-1}^t \\ \rho_i^t \\ \rho_{i+1}^t \end{pmatrix} + w \quad (\text{III.4})$$

In the next section, we will see that the decomposition in “modes” as shown in Table III.1 leads to a piecewise affine formulation of the Godunov scheme in the case of the triangular flux function.

B. Polyhedral piecewise affine formulation of the Godunov scheme

Let us consider a link with discrete time step indexed by $t \geq 0$ and discrete space step indexed by $i = 1, \dots, n$, and let us denote $\rho^t = (\rho_0^t, \rho_1^t, \dots, \rho_n^t, \rho_{n+1}^t)$ an $n + 2$ dimensional vector which describes the state of the link at time t in the space $\mathcal{S} = [0, \rho_{\text{jam}}]^{n+2}$, where ρ_i^t is the density at time t and cell i . We can note that the ghost cells 0 and

$n + 1$ are included in the state of the link.³

Definition of the space of modes: Let us denote by \mathcal{M}_n the space of modes of the system ($\mathcal{M}_n \subset \{1, \dots, 7\}^n$, see Table III.1). For $\mathbf{m} \in \mathcal{M}_n$, \mathbf{m} is a vector of dimension n for which the i -th entry $m_i \in \{1, \dots, 7\}$ is the mode at cell i . Equivalently, each element of \mathcal{M}_n can be described as a sequence of regions in which the pair (ρ_i, ρ_{i+1}) is, for $i = 0, \dots, n$. Hence, we define the equivalent space of modes $\tilde{\mathcal{M}}_n \subset \{w, l, d\}^{n+1}$, and for $\mathbf{s} \in \tilde{\mathcal{M}}_n$, \mathbf{s} is a vector of dimension $n + 1$ for which the i -th entry s_i is equal to l if $(\rho_i, \rho_{i+1}) \in \mathbf{L}$, for $i = 0, \dots, n$. As will be seen later, this second definition gives a description of the *partition of the space \mathcal{S} into different polyhedra \mathbf{P}_m in which the mode is \mathbf{m}* . See Figure III.1 for an illustration.

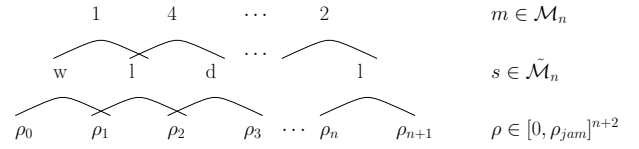


Fig. III.1: An illustration of the vectors $\rho \in [0, \rho_{\text{jam}}]^{n+2}$, $\mathbf{s} \in \tilde{\mathcal{M}}_n \subset \{w, l, d\}^{n+1}$, and $\mathbf{m} \in \mathcal{M}_n \subset \{1, \dots, 7\}^n$ for n cells.

The n -dimensional vector $\mathbf{m} \in \mathcal{M}_n$ describes the mode of the link at any time, as defined in the previous section. At each time step, the state of the link is updated through the following nonlinear dynamical system:

$$\rho^{t+1} = F_{\mathbf{m}}[\rho^t] \quad \text{if } \rho^t \in \mathbf{P}_{\mathbf{m}} \quad (\text{III.5})$$

with $F_{\mathbf{m}}[\cdot]$ an $n + 2$ dimensional function vector, and \mathbf{m} the mode at time t . With u^t and d^t the boundary conditions upstream and downstream at time step t , the i -th entry $\rho_i^{t+1} = F_{\mathbf{m}, i}[\rho^t]$ is:

$$\rho_i^{t+1} = \begin{cases} f_{m_i}(\rho_{i-1}^t, \rho_i^t, \rho_{i+1}^t) & \text{for } i = 1, \dots, n \\ u^t & \text{for } i = 0 \\ d^t & \text{for } i = n + 1 \end{cases} \quad (\text{III.6})$$

where m_i denotes the i -th entry of $\mathbf{m} \in \mathcal{M}_n$, i.e. the mode of cell i at time step t , and $f_{m_i}(\rho_{i-1}^t, \rho_i^t, \rho_{i+1}^t)$ is the m_i -th entry of the function vector f evaluated at $(\rho_{i-1}^t, \rho_i^t, \rho_{i+1}^t)$. We note that $\rho_0^{t+1} = u^t$ and $\rho_{n+1}^{t+1} = d^t$, which means that the ghost cells are the boundary conditions of the Godunov scheme. For a triangular flux function, with L_{m_i} the m_i -th line of J_T and w_{m_i} the m_i -th entry of w , the update operator of the dynamical system is:

³The values of ρ_0^t and ρ_{n+1}^t are given by the prescribed boundary conditions to be imposed on the in left and right side of the domain respectively. Note that these boundary values do not always affect the physical domain because of the nonlinear operator (II.10), which causes the boundary conditions to be implemented in the weak sense. For more details, see [32] and [25].

$$\rho_i^{t+1} = \begin{cases} L_{m_i} \cdot \begin{pmatrix} \rho_{i-1}^t \\ \rho_i^t \\ \rho_{i+1}^t \end{pmatrix} + w_{m_i} & \text{for } i = 1, \dots, n \\ u^t & \text{for } i = 0 \\ d^t & \text{for } i = n + 1 \end{cases} \quad (\text{III.7})$$

When $\rho^t \in \mathbf{P}_m$, the $(n+2) \times (n+2)$ -dimensional state-transition matrix A_m is obtained by concatenating the 3×1 row vectors L_{m_i} along the diagonal. It is tridiagonal with diagonal elements $\{0, J_{m_1,2}, \dots, J_{m_n,2}, 0\}$, lower diagonal elements $\{J_{m_1,1}, J_{m_2,1}, \dots, J_{m_n,1}, 0\}$, and upper diagonal elements $\{0, J_{m_1,3}, J_{m_2,3}, \dots, J_{m_n,3}\}$ where J (or J_T) are defined in equations (III.2), (III.3). Equivalently:

$$A_m = \begin{pmatrix} 0 & \dots & 0 \\ L_{m_1} & & \\ & \ddots & \\ & & L_{m_n} \\ 0 & \dots & 0 \end{pmatrix} \quad (\text{III.8})$$

Let us denote b_m and c_t the two vectors of dimension $(n+2)$ with entries $\{0, w_{m_1}, \dots, w_{m_n}, 0\}$ and $\{u^t, 0, \dots, 0, d^t\}$ respectively, and \mathbf{P}_m the subset of space \mathcal{S} where the mode is m . The update operator of the dynamical system is *piecewise affine*:

$$\rho^{t+1} = A_m \rho^t + b_m + c^t \quad \text{if } \rho^t \in \mathbf{P}_m \quad (\text{III.9})$$

We now provide a description of the partition of the space into the polyhedra \mathbf{P}_m in which the mode is m . Note that in this formula, $A_m \rho^t$ represents the local (affine) discretization of the PDE, and c_t the boundary condition.

Polyhedral partition of the space: For a discretization into n cells, we chose to describe the ensemble of modes $\tilde{\mathcal{M}}_n$ in sequences $s \in \{w, l, d\}^{n+1}$ and define \mathbf{P}_s the corresponding polyhedron for each sequence. Let us define 3^{n+1} polyhedra \mathbf{W}_i , \mathbf{L}_i , and \mathbf{D}_i for $i = 0, \dots, n$ in the space \mathcal{S} obtained by instantiating $h(\rho_1)$ with (II.12):

$$\begin{aligned} \mathbf{W}_i &= \{(\rho_i, \rho_{i+1}) \mid \rho_{i+1} + \frac{v_f}{\omega_f} \rho_i > \rho_{\text{jam}}, \rho_{i+1} > \rho_c\} \\ \mathbf{L}_i &= \{(\rho_i, \rho_{i+1}) \mid \rho_i > \rho_c, \rho_{i+1} \leq \rho_c\} \\ \mathbf{D}_i &= \{(\rho_i, \rho_{i+1}) \mid \rho_{i+1} + \frac{v_f}{\omega_f} \rho_i \leq \rho_{\text{jam}}, \rho_i \leq \rho_c\} \end{aligned} \quad (\text{III.10})$$

The polyhedron \mathbf{P}_s , in which the mode is $s \in \tilde{\mathcal{M}}_n$, can be described as an intersection of $n+1$ polyhedra \mathbf{Q}_i :

$$\mathbf{P}_s = \bigcap_{i=0}^n \mathbf{Q}_i \quad \text{with} \quad \mathbf{Q}_i = \begin{cases} \mathbf{W}_i & \text{if } s_i = w \\ \mathbf{L}_i & \text{if } s_i = l \\ \mathbf{D}_i & \text{if } s_i = d \end{cases} \quad (\text{III.11})$$

Moreover, for two different modes s and s' , and corresponding polyhedra $\mathbf{P}_s = \bigcap_{i=0}^n \mathbf{Q}_i$ and $\mathbf{P}_{s'} = \bigcap_{i=0}^n \mathbf{Q}'_i$, we

can find an index i for which \mathbf{Q}_i and \mathbf{Q}'_i are disjoint. For instance, suppose without loss of generality that $\mathbf{Q}_i = \mathbf{W}_i$ and $\mathbf{Q}'_i = \mathbf{D}_i$, and we know that \mathbf{W}_i and \mathbf{D}_i are disjoint. Then in this case, the hyperplane $\{\rho \mid \rho_{i+1} + \frac{v_f}{\omega_f} \rho_i = \rho_{\text{jam}}\}$ is a separating hyperplane between \mathbf{P}_s and $\mathbf{P}_{s'}$. Hence, \mathbf{P}_s and $\mathbf{P}_{s'}$ are disjoint and the family $\{\mathbf{P}_s\}_{s \in \tilde{\mathcal{M}}_n}$ is a partition of $\tilde{\mathcal{M}}_n$.

IV. HYBRID KALMAN FILTERING ESTIMATION

The Kalman filter provides the state estimate and the covariance estimate given the sequence of measurements $\mathbf{y}^{0:t}$, and a sequence of control parameters. We now present a simple *Hybrid Kalman filtering* estimation algorithm based on the Kalman filter in the estimated affine mode \hat{m} of the Godunov scheme with n cells, as explicitly derived in section III-A. Note that the state at time t is $\rho^t = (\rho_0^t, \rho_1^t, \dots, \rho_n^t, \rho_{n+1}^t)$, a vector of dimension $n+2$ that includes the two ghost cells 0 and $n+1$ which are the boundary conditions.

Remark: The application of the Kalman filter in each mode is in practice equivalent to the *extended Kalman filter*. Since the dynamical system is linear in each mode, the linearization of the Godunov scheme is equal to the system itself. However, the Jacobian is piecewise constant and has discontinuities at the boundaries between modes, where the Godunov scheme is not differentiable. The boundaries of the polyhedra are labeled to one of the polyhedra they bound as in (III.10), where there are strict inequalities on one side and non-strict inequalities on the other. This assumes that the polyhedra are a true partition of the space.

A. Kalman filtering algorithm

In order to use the *Kalman filter* to estimate the state of the link given a sequence of noisy observations, we model the process by adding a white noise to the underlying dynamical system model. The “true” state at time $t+1$, namely ρ^{t+1} , is then given by the update equation:

$$\rho^{t+1} = A_m \rho^t + b_m + c^t + \eta^t \quad \text{if } \rho^t \in \mathbf{P}_m \quad (\text{IV.1})$$

where $\eta^t \sim N(0, Q^t)$ is the Gaussian zero-mean, white state noise with covariance Q^t . To apply the *control update* of the Kalman filter, it is then necessary to know the mode m of the state ρ^t (i.e. m such that \mathbf{P}_m).

Additionally, the observation model for the link is given by:

$$\mathbf{y}^t = H^t \rho^t + \chi^t \quad (\text{IV.2})$$

where $H^t \in \{0, 1\}^{p^t \times n}$ is the linear observation matrix which encodes the p^t observations (each one of them being at a discrete cell on the highway) for which the density is observed⁴during discrete time step t , and n is the number of cells along the link. The last term in equation (IV.2) is

the white, zero mean observation noise $\chi^t \sim N(0, R^t)$ with covariance matrix R^t .

Let $\hat{\rho}^{t:t}$ and $P^{t:t}$ be the *a posteriori* state estimate and error covariance matrix at time t , and \hat{m} the mode estimate. Then the *predicted* state estimate $\hat{\rho}^{t+1:t}$ and covariance estimate $P^{t+1:t}$ of the *prediction step* are:

$$\begin{aligned} \hat{\rho}^{t+1:t} &= A_{\hat{m}} \hat{\rho}^{t:t} + b_{\hat{m}} + c^t \text{ if } \hat{\rho}^{t:t} \in \mathbf{P}_{\hat{m}} \\ P^{t+1:t} &= A_{\hat{m}} P^{t:t} (A_{\hat{m}})^T + Q^t \end{aligned} \quad (\text{IV.3})$$

The *measurement residual* r^{t+1} , *residual covariance* S^{t+1} , *Kalman gain* K^{t+1} , *updated state estimate* $\hat{\rho}^{t+1:t+1}$, and *updated estimate covariance* P^{t+1} of the *update step* are:

$$\begin{aligned} r^{t+1} &= y^{t+1} - H^{t+1} \hat{\rho}^{t+1:t} \\ S^{t+1} &= H^{t+1} P^{t+1:t} (H^{t+1})^T + R^{t+1} \\ K^{t+1} &= P^{t+1:t} (H^{t+1})^T (S^{t+1})^{-1} \\ \hat{\rho}^{t+1:t+1} &= \hat{\rho}^{t+1:t} + K^{t+1} r^{t+1} \\ P^{t+1:t+1} &= (I - K^{t+1} H^{t+1}) P^{t+1:t} \end{aligned} \quad (\text{IV.4})$$

B. Implementation and complexity

Since the number of modes grows exponentially as the number of cells increases (see Appendix VIII), it is computationally expensive to store a matrix $A_{\hat{m}}$ for each mode \hat{m} . Fortunately, it is possible to compute the *predicted state estimate* $\hat{\rho}^{t+1:t}$ and the *predicted covariance estimate* $P^{t+1:t}$ in linear time and quadratic time respectively, without forming any dense matrix $A_{\hat{m}}$. This relies on the tridiagonality of $A_{\hat{m}}$ and the homogeneity of the segment of road considered, which requires to store only the seven possible modes at each cell.⁵

In particular, equation (III.7) gives a simple procedure to compute $\hat{\rho}^{t+1:t} = F_{\hat{m}}[\hat{\rho}^{t:t}]$ in linear time from $\hat{\rho}^{t:t}$, J_T , w , c^t , and \hat{m} such that $\hat{\rho}^{t:t} \in \mathbf{P}_{\hat{m}}$.

The double product $A_{\hat{m}} P^{t:t} (A_{\hat{m}})^T$ can be computed in quadratic time from $P^{t:t}$ and J_T . With the entries of $A_{\hat{m}} P^{t:t}$ indexed from 0 to $n+1$:

$$(A_{\hat{m}} P^{t:t})_{i,j} = \begin{cases} L_{\hat{m}_i} \cdot \begin{pmatrix} p_{i-1,j} \\ p_{i,j} \\ p_{i+1,j} \end{pmatrix} & \text{if } (i,j) \in \{1, \dots, n\}^2 \\ 0 & \text{otherwise} \end{cases} \quad (\text{IV.5})$$

where $L_{\hat{m}_i}$ is the \hat{m}_i -th row of J_T , \hat{m}_i the i -th entry of \hat{m} , and $p_{i,j}$ is the entry (i,j) -th entry of $P^{t:t}$. And the computation of the second matrix multiplication with entries indexed from 0 to $n+1$ is:

⁴A data-cleaning scheme is designed based on the causes of errors in loop detectors data deployed by PeMS (<http://pems.dot.ca.gov>). The raw data is then converted into density $\rho_i^t = o_i^t / g_i^t$ where the occupancy o_i^t is the fraction of time a reference point is occupied in cell i at time t and the g-factor g_i^t is the average length of vehicle crossing this point. For more information, see <http://traffic.berkeley.edu>.

⁵In the case of a heterogeneous road (i.e. a different flux function for each cell), up to all nine possible local modes for each cell have to be stored, which is still bound by $9 \times n$, where n is the number of cells.

$$\begin{aligned} &(A_{\hat{m}} P^{t:t} (A_{\hat{m}})^T)_{i,j} \\ &= \begin{cases} (q_{i,j-1} \ q_{i,j} \ q_{i,j+1}) \cdot L_{\hat{m}_j}^T & \text{if } (i,j) \in \{1, \dots, n\}^2 \\ 0 & \text{otherwise} \end{cases} \end{aligned} \quad (\text{IV.6})$$

where $q_{i,j}$ is the entry (i,j) -th entry of $A_{\hat{m}} P^{t:t}$. We can note that the first line and first column of $P^{t:t}$ have only zero elements because the boundary condition $\hat{\rho}_0^t = u^t$ is deterministic (i.e. $\text{cov}(u^t, \hat{\rho}_i^t) = 0$ for $i = 1, \dots, n$), and similarly the last line and last column of P^t are null since the boundary condition $\hat{\rho}_{n+1}^t = d^t$ is deterministic.

The three equations (III.7, IV.5, IV.6) show that both time complexity and space complexity of the *prediction step* are $O(n^2)$.

C. Mathematical analysis

Estimation of the mode: Contrary to other models [14], [21] in which the transition from the mode at time t to the one at time $t+1$ follows a Markov model, the mode in our model is obtained by finding the polyhedron \mathbf{P}_m such that $\hat{\rho}^{t:t} \in \mathbf{P}_m$ (see update equation (IV.1)). This is simply a reformulation of the Godunov scheme as seen in Section III and the choice of this deterministic model relies on the assumption that the Godunov scheme is a good physical model for traffic estimation.

Gaussian assumption: In the *hybrid Kalman filter* (H-KF), a Kalman filter is applied to the mode given by the update equation (IV.1). Specifically, we assume here that the system of linear equations of the current mode holds for the whole space \mathcal{S} , in which case the Gaussian assumption is valid for the updated state. In reality, the model is piecewise affine and such a transformation on a Gaussian distribution yields a mixture of truncated Gaussians, which does not have a practical analytical formula.

V. NUMERICAL RESULTS

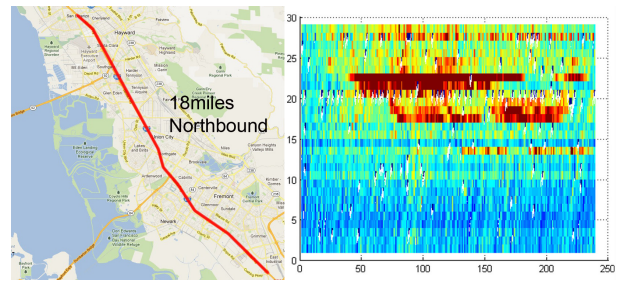


Fig. V.1: Left: experimental data location: 18-mile long stretch of I-880 in the Bay Area on the *Mobile Century* site. Right: contour plot of the density from the 29 PeMS stations (Y-axis) every 30s (X-axis).

In this section, we implement the density-based Godunov scheme on an 18-mile section of I-880 Northbound in the Bay Area, California (Figure V.1) combined with the hybrid Kalman filtering presented in section IV. We use density measurements along the I-880 from 29 loop detectors (PeMS) every 30s on March 5th, 2012 between 7am and 8am to compute density values and integrate them in the model. Each cell has a length of 198m and the time step is 5s. The

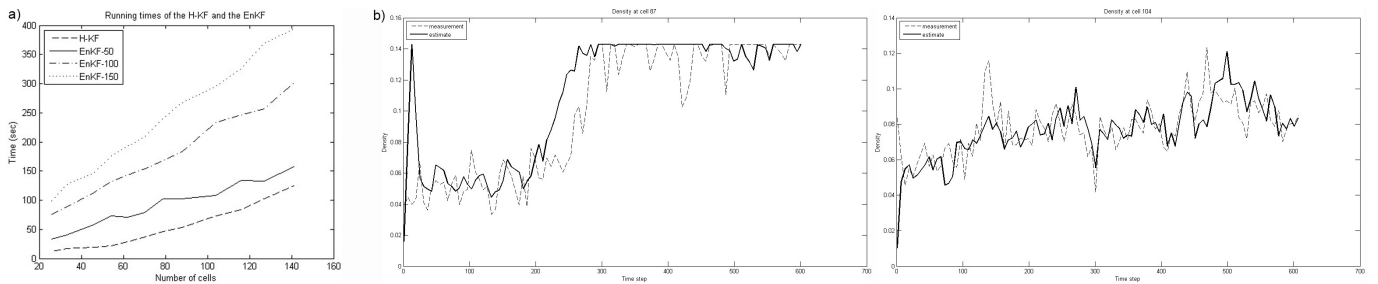


Fig. V.2: a) Computational time for an increasing section of the I-880 (measured in the number of cells) for the H-KF (dashed line), the EnKF with 50 ensembles (continuous line), the EnKF with 100 ensembles (dashed-dotted line), and the EnKF with 150 ensembles (dotted line). b) Comparison between the density measurements (dashed line) and estimates (bold line) at one cell. Top: at cell 87, bottom: at cell 104.

output of the model is compared with the *Ensemble Kalman filtering* (EnKF) with 100 ensembles, which is commonly used in the traffic monitoring community [32].

A. Computational time

The running times of the implementation of both the H-KF and the EnKF estimators on an Intel® Core™ i5 480M 2.67GHz are shown in Figure V.2 a, for increasing portions of the I-880 starting from East Industrial in Fremont, CA (60 cells (~7.5miles) span from East Industrial to Dumbarton Bridge, and 113 cells (~14miles) reaches San Mateo Bridge).

Mandel’s report [20] shows that the total computational complexity of the EnKF algorithm is $O(m^3 + m^2N + mN^2 + nN^2)$ where n is the dimension of the state, m the number of observations and N the number of ensembles. A similar analysis shows that the computational complexity of the H-KF is $O(mn^2 + m^3 + nm^2)$. As the density measurements along the highway are sparse (i.e. $m \ll n, N$), the computational complexities become $O(N^2 + nN^2)$ and $O(n^2)$ for the EnKF and the H-KF respectively. The time complexities of the EnKF and the H-KF are roughly *linear* and *quadratic* in the dimension n respectively. However, when N is fixed and n increases, the constant term in $N^2 + nN^2$ is large, which explains the large relative difference between both running times when n is small (cf Figure V.2 a). When n is large, the EnKF performs better.

B. Output of the Hybrid Kalman filtering estimation

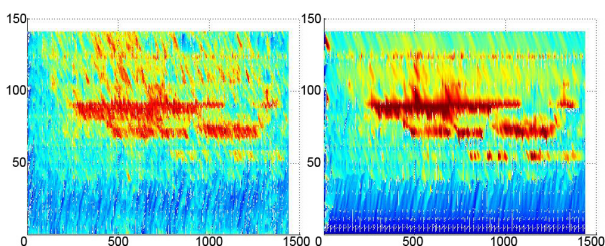


Fig. V.3: Output of the EnKF (left) and the hybrid Kalman filtering (right) on the I-880. The time step is on the X-axis and the number of cells is on the Y-axis.

Figure V.3 shows the contour plot of the output of the EnKF and the H-KF estimators, which consists in the density in the time-space domain. The regions with high density are represented in red and the regions with low density in

blue. Both estimators give similar higher resolution scalar fields of the density (1440 time steps by 141 cells) by assimilating sparse density measurements (240 time steps by 29 PeMS stations, cf Figure V.1). Moreover, by removing measurements at an arbitrary cell, Figure V.2 b empirically shows that the estimation algorithm performs well since the density estimate is close to the actual measurement.

VI. CONCLUSION AND FUTURE WORK

In this work we considered the *Godunov scheme* for the discretization of the so-called *Lighthill-Whitham-Richards* equation with a triangular diagram for the state estimation of discretized hyperbolic scalar partial differential equations.

Assuming the parameters are the same for each cell of the discretized model, we have shown that the space of all states can be decomposed into polyhedra in which the nonlinear dynamical system can be expressed in *affine* form. We have also provided a description of the modes: their number grows exponentially as the dimension increases, and each one of them can be represented as an intersection of a linear number of *half-spaces*.

We have applied a basic form of *hybrid Kalman filtering* to demonstrate some computational capabilities enabled by the *piecewise affine* decomposition. Despite some approximations in the estimation of the mode and in the Gaussian assumption, the statistical filter performs well on the running time and on the accuracy of the estimation. This motivates the application of filters which are more tuned to the actual piecewise affine system such as a *multiple mode KF*, or an *interacting multiple mode KF*.

VII. ACKNOWLEDGEMENTS

The authors would like to thank the members of the staff of the California Institute for Innovative Transportation for its contributions to develop, build, and deploy the system infrastructure of *Mobile Millennium* on which this article relies.

VIII. APPENDIX

Suppose that the pair (ρ_0, ρ_1) is in the region **W**, then the list of possible combinations in Table III.1 shows that (ρ_1, ρ_2) can be either in **W** or **L**. Similarly, if (ρ_0, ρ_1) is in the region **L**, (ρ_1, ρ_2) can be either in **W** or **L**, and for (ρ_0, ρ_1) in **D**, (ρ_1, ρ_2) can be either in **W**, **L**, or **D**. As an example, figure VIII.1 describes all the possible sixteen combinations for the first three pairs (ρ_0, ρ_1) , (ρ_1, ρ_2) , and (ρ_2, ρ_3) .

We can recursively compute the number of “modes” M_k with respect to k , where k is the number of cells of the discretized link. Let us denote by w_k , l_k , and d_k the number of modes for which (ρ_k, ρ_{k+1}) is in **W**, **L**, and **D** respectively ($n_k = w_k + l_k + d_k$). Then we have these equations:

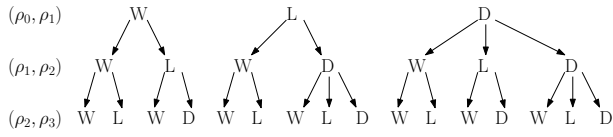


Fig. VIII.1: The sixteen possible modes for the first three pairs (ρ_0, ρ_1) , (ρ_1, ρ_2) , and (ρ_2, ρ_3) .

$$\begin{aligned} w_0 &= l_0 = d_0 = 1 \\ w_{k+1} &= w_k + l_k + d_k \\ l_{k+1} &= w_k + d_k \\ d_{k+1} &= l_k + d_k \end{aligned} \quad \text{for } k \geq 0 \quad (\text{VIII.1})$$

Using matrix notations and equation (VIII.1):

$$\begin{bmatrix} w_k \\ l_k \\ d_k \end{bmatrix} = A^k \times \begin{bmatrix} w_0 \\ l_0 \\ d_0 \end{bmatrix} \quad \text{where } A = \begin{bmatrix} 1 & 1 & 1 \\ 1 & 0 & 1 \\ 0 & 1 & 1 \end{bmatrix} \quad (\text{VIII.2})$$

It is possible to compute A^k explicitly by diagonalizing the matrix A , to obtain an explicit expression for w_k , l_k , and d_k in the form of $a \cdot \beta^k + b \cdot \gamma^k + c \cdot \delta^k$. However, this analytical expression is unwieldy, so we will just derive lower and upper bounds to n_k . It can be proved that $d_k \leq n_k/2$ for $k \geq 0$, then we can prove recursively that $3 \cdot 2^k \leq n_k \leq 3 \cdot (2.5)^k$.

number of cells	1	2	5	10	20
number of modes	7	16	182	10426	34206521
bound without analysis	7	49	16807	282475249	$8 \cdot 10^{16}$

TABLE VIII.1: Number of modes for a homogeneous road.

Even if we have found the minimal polyhedral partition of the space, the number of modes grows exponentially as the number of cells increases, so it is difficult to store all the possible modes. However, at any time step, the mode of each cell can be determined among the 7 possible modes and constructed sequentially building up the general mode of the segment of road.

REFERENCES

- [1] K. Agyemang-Duah and F. Hall. Some issues regarding the numerical value of freeway capacity. *International Symposium on Highway Capacity*, 1991.
- [2] A. Balluchi, L. Benvenuti, M. D. di Benedetto, C. Pinello, and A. L. Sangiovanni-Vincentelli. Automotive engine control and hybrid systems: challenges and opportunities. *Proc. IEEE*, 88 (7):888–912, 2000.
- [3] M. Cassidy and R. Bertini. Some traffic features at freeway bottle-necks. *Transportation Research*, 33:25–42, 1999.
- [4] C. Chen, P. Varaiya, and J. Kwon. An empirical assessment of traffic operations. *16th International Symposium on Transportation and Traffic Theory*, pages 105–123, 2005.
- [5] Rong Chen and Jun S. Liu. Mixture Kalman filters. *Royal Statistical Society*, 62:493–508, 2000.
- [6] C. F. Daganzo. The cell transmission model: a dynamic representation of highway traffic consistent with the hydrodynamic theory. *Transportation Research Part B* 28, no. 4, 28:269–287, 1994.
- [7] C. F. Daganzo. The cell transmission model, part II: Network traffic. *Transportation Research Part B* 29, no. 2, 29:79–93, 1995.
- [8] M. Garavello and B. Piccoli. *Traffic Flow on Networks*. American Institute of Mathematical Sciences, 2006.
- [9] D. Gazis and C. Knapp. On-line estimation of traffic densities from time-series of flow and speed data. *Transp. Sci.*, 5 (3):283–301, 1971.
- [10] E. Godlewski and P-A. Raviart. *Numerical approximation of hyperbolic systems of conservation laws*. Applied Mathematical Sciences, 1996.
- [11] S.K. Godunov. A finite difference method for the numerical computation of discontinuous solutions of the equations of fluid dynamics. *Math. Sbornik*, 47:271–306, 1959.
- [12] B. D. Greenshields. A study of traffic capacity. *Proceedings of the 14th annual meeting of the Highway Research Board*, 14:448–477, 1934.
- [13] F. Hall and K. Agyemang-Duah. Freeway capacity drop and the definition of capacity. *Transportation Research Record*, pages 91–98, 1991.
- [14] I. Hwang, H. Balakrishnan, and C. Tomlin. State estimation for hybrid systems: applications to aircraft tracking. *IEE Proc. Control Theory and Applications*, 153(5):556–566, Sep. 2006.
- [15] J. P. Lebacque. The Godunov scheme and what it means for first order traffic flow models. *13th International Symposium on Transportation and Traffic Theory*, pages 647–77, 1996.
- [16] M. D. Lemmon, K. X. He, and I. Markovsky. Supervisory hybrid systems. *IEEE Control Systems Magazine*, 19 (4):42–55, 1999.
- [17] B. Lennartson, M. Tittus, B. Egardt, and S. Pettersson. Hybrid systems in process control. *IEEE Control Systems Magazine*, 16 (5):45–56, 1996.
- [18] R. J. LeVeque. *Numerical Methods for Conservation Laws*. Birkhuser Basel, 1992.
- [19] M. J. Lighthill and G. B. Whitham. On Kinematic Waves II. A Theory of Traffic Flow on Long Crowded Roads. *Proceedings of the Royal Society of London. Series A, Mathematical and Physical Sciences*, 229:317–345, 1955.
- [20] J. Mandel. Efficient Implementation of the Ensemble Kalman Filter. *CCM Report No. 231*, 2006.
- [21] L. Munoz, X. Sun, R. Horowitz, and Luis Alvarez. Traffic Density Estimation with the Cell Transmission Model. *Proceedings of the American Control Conference*, pages 3750–3755, June 2003.
- [22] M. Papageorgiou, J.-M. Bloussville, and H. Hadj-Salem. Modelling and real-time control of traffic flow on the southern part of Boulevard Peripherique in Paris: Part I: Modelling. *Transportation Research*, 24 (5):345–359, 1990.
- [23] P. I. Richards. Shock Waves on the Highway. *Operations Research*, 4:42–51, 1956.
- [24] T. Schreiter, C. van Hinsbergen, F. Zuurbier, H. van Lint, and S. Hoogendoorn. Data-model synchronization in extended Kalman filters for accurate online traffic state estimation. *2010 Proceedings of the Traffic Flow Theory Conference, Annecy, France*, 2010.
- [25] I. S. Strub and A. M. Bayen. Weak formulation of boundary conditions for scalar conservation laws: an application to highway traffic modeling. *Int. J. Robust Nonlinear Control*, 16:733–748, 2006.
- [26] M. Szeto and D. Gazis. Application of Kalman filtering to the surveillance and control of traffic systems. *Transp. Sci.*, 6 (4):419–439, 1972.
- [27] C. Tomlin, G. Pappas, and S. Sastry. Conflict resolution for air traffic management: A study in multiagent hybrid systems. *IEEE Trans. Autom. Control*, 43 (4), 1998.
- [28] Y. Wang and M. Papageorgiou. Real-time freeway traffic state estimation based on extended Kalman filter: a general approach. *Transportation Research*, 39 (2):141–167, 2005.
- [29] Y. Wang and M. Papageorgiou. Real-time freeway traffic state estimation based on extended Kalman filter: A case study. *Transp. Sci.*, 41 (2):167, 2007.
- [30] D. B. Work and A. M. Bayen. Impacts of the mobile internet on transportation cyber-physical systems: Traffic monitoring using smartphones. *National Workshop for Research on High-Confidence Transportation Cyber-Physical Systems: Automotive, Aviation, & Rail*, 2008.
- [31] D. B. Work, A. M. Bayen, and Q. Jacobson. Automotive cyber-physical systems in the context of human mobility. *National Workshop on High-Confidence Automotive Cyber-Physical Systems*, 2008.
- [32] D. B. Work, S. Blandin, O. Tossavainen, B. Piccoli, and A. M. Bayen. A Traffic Model for Velocity Data Assimilation. *Applied Mathematics Research eXpress*, 2010.